ELSEVIER

Journal of Power Sources 87 (2000) 39–56

JOURNAL OF POWER SOURCES

www.elsevier.com/locate/jpowsour

Influence of fast charge on the life cycle of positive lead–acid battery plates

D. Pavlov [a,*], G. Petkova [a], M. Dimitrov [a], M. Shiomi [b], M. Tsubota [b]

[a] *Central Laboratory of Electrochemical Power Sources, 1113 Sofia, Bulgaria*
[b] *Japan Storage Battery, Kyoto, Japan*

Received 23 December 1998; received in revised form 15 July 1999; accepted 19 August 1999

Abstract

A criterion has been found for determination of the factor limiting the discharge of the lead dioxide plate. When on discharge with moderate currents, an arrest or a shoulder appears between 1.0 and 0.7 V (vs. $Hg/HgSO_4$ electrode) in the potential transient, then the charging potential transient features a peak at the beginning of the curve. The capacity is limited by the interface. The life cycle of the battery is short. This phenomenon is known as PCL effect. When a broad maximum occurs in the potential transient on charge, this indicates that the electrode capacity is limited by zones of high resistance in positive active mass (PAM) near the interface. The capacity is determined by the lead dioxide active mass. It has been established that the life of the positive plate is proportional to the current density during the initial charge stage. A sol–gel–crystal mechanism of the charge processes is proposed to explain this effect of fast charge on electrode life. The high rate of the electrochemical reaction leads to high oversaturations of the $Pb(OH)_4$ sol and to fast formation of gel–crystal $PbO(OH)_2/PbO_2$ particles, which not only form new agglomerates tightly connected to the PAM skeleton, but also fill in and improve the contacts between the agglomerates. The latter process has the effect of ''welding'' of the PAM skeleton. Moreover, the higher concentration of the $Pb(OH)_4$ sol affects the macro- and microstructure of the PAM, which in turn has an influence on the electrochemical reaction. Impedance measurements have evidenced different values of the electron transfer resistance in electrodes charged at high and low currents.

Keywords: Lead–acid batteries; Charging of lead–acid batteries; Fast charge; PCL effect; Influence of Sb on the PCL effect; Mechanism of fast charge processes

1. Introduction

It has been established that the capacity and life cycle of the lead–acid battery depend on the charge current. The high rate recharge has a beneficial effect on battery capacity [1]. It is assumed that the positive effect of high-rate recharge is due to the properties of the positive active mass (PAM) rather than being an effect of a special type of electrode design or grid alloy or structure of the interface grid/PAM [2–8]. The agglomerate-of-spheres model (AOSM) has been proposed to explain the above phenomena [9]. Recently, it has been found that when the battery is charged with a strong current during the first stage, its life cycle is longer [10–12]. The same effect has been observed when pulse charge current is applied [13].

Despite the great number of publications, it is not quite clear yet what are the phenomena responsible for this improvement in battery life on fast charge and in which part of the structure of the positive plate do these phenomena occur. The basic aim of the present paper is to search for answers to these questions.

2. Experimental methods

2.1. Electrode construction

In order to distinguish between the phenomena proceeding in the PAM and at the interface, we designed a special model bi-electrode (MBE). A conceptual scheme of its construction is presented in Fig. 1. This MBE is an analogue of the double-grid plates developed by us earlier [14].

* Corresponding author. Tel.: +359-2-718651; fax: +359-2-731552; e-mail: dpavlov@mbox.cit.bg

0378-7753/00/$ - see front matter
PII: S0378-7753(99)00358-4

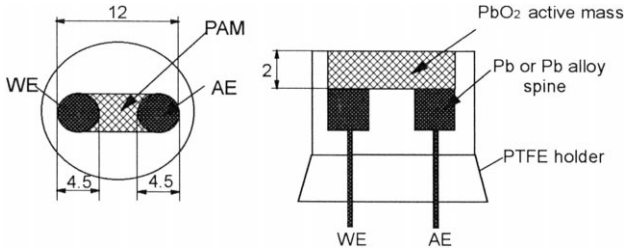

Fig. 1. MBE construction. Dimensions are in millimeter.

The MBE consists of two cylindrical lead spines (used as substrates) inserted into a Teflon holder with their bases covered with a common layer of PAM. Its weight is 0.41 g. The PAM is obtained from $4PbO \cdot PbSO_4$ (4BS) or $3PbO \cdot PbSO_4 \cdot H_2O$ (3BS) pastes. One of the spines serves as a working electrode (WE) and the other one is an auxiliary electrode (AE).

The following spine combinations were used for the MBE:

1. Pb–1.2% Sn–0.06% Ca||Pb–1.2% Sn–0.06% Ca|PAM (4BS or 3BS) — symmetrical MBE
2. Pb–1.2% Sn–0.06% Ca||Pb–1.5% Sb–0.2% Sn|PAM (4BS or 3BS) — asymmetrical MBE

The MBE is cycled through the WE first. If after the discharge through the WE, the PAM can still deliver capacity through the AE, this indicates that the interface has limited the MBE capacity. If no residual capacity can be delivered by the AE, this is an indication that the structure and properties of the PAM have limited the capacity.

The results obtained at 5-h rate of discharge of the PAM through the WE or through the AE, or through both spines when short-circuited are summarised in Table 1. Practically, the whole PAM is involved in the discharge irrespective of the spine through which the discharge is conducted.

2.2. Experimental set up and testing mode

Life cycle tests were performed with a classical three-electrode cell presented schematically in Fig. 2.

RE is a Hg/Hg_2SO_4 reference electrode. All potential measurements in this study were performed vs. this reference electrode. CE is a small lead plate used as a counter electrode. Electrode charge and discharge were carried out by using a MSTAT-4 + system (ARBIN INSTRUMENTS).

Table 1
Electrode capacity when discharged through the WE or through the AE or through both spines when short circuited

	5-h rate of discharge		
	WE + AE	WE PbSnCa	AE PbSnSb
mA h/g	98.28	96.48	97.80
PAM utilization (%)	43.8	43.1	43.7

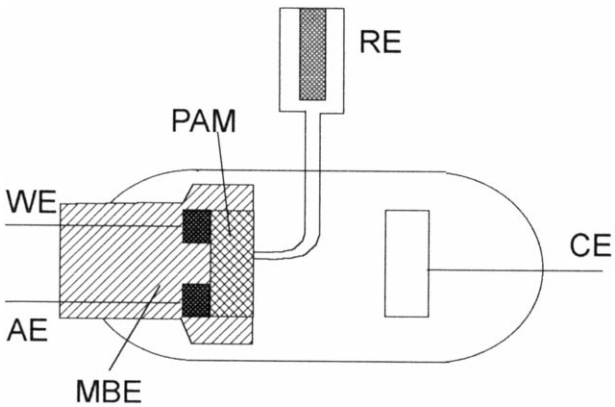

Fig. 2. Schematic representation of the electrochemical cell used for the investigations. RE is a Hg/Hg_2SO_4 reference electrode, CE is a small Pb plate with NAM.

After formation of the electrodes, they were subjected to four preparatory cycles comprising 10 h of charge and 10 h of discharge. Then the cycling tests proper started.

The electrodes were charged employing a two-step constant current–constant potential regime. Constant current I_1 was maintained until the electrode potential reached 1.45 V. Charging was continued at a constant potential $E_2 = 1.45$ V until a charge factor $F_{ch} = 110\%$ was reached. To study the influence of initial charging current, three different ranges were tested: $I_1 = 0.2C_0$, $0.5C_0$, $1.5C_0$ A. The discharge was conducted always at constant current of 25 mA/g active mass, to a cut-off potential 0.7 V (100% DOD).

After a definite number of cycles, some of the electrodes were subjected to impedance measurements. They were performed after discharge of the WE and/or the AE down to a potential of 0.7 V. The potential of the MBE was then maintained equal to 0.7 V and the impedance spectra were recorded by using a SOLARTRON 1288/1250 system in the frequency range from 65 kHz to 0.01 Hz, with signal amplitude 5 mV.

3. Experimental results

3.1. Influence of charging current on the life cycle of the lead dioxide electrode

The capacity vs. cycle number curves for symmetrical electrodes are presented in Fig. 3a and for asymmetrical ones in Fig. 3b, both produced with 4BS paste of density 4.1 g/cm^3. As the initial electrode potential at $I_1 = 1.5C_0$ A was higher than 1.45 V, the potential limiting condition ($E_2 = 1.45$ V) did not hold for the first 10 min. After that, the electrode was charged at a constant potential of 1.45 V.

The following conclusions can be drawn from the data in Fig. 3.

On increasing the charging current from 0.2 to $1.5C_0$ A, the life of the electrode is more than doubled. The beneficial effect of fast charge is reported in Refs. [1–13].

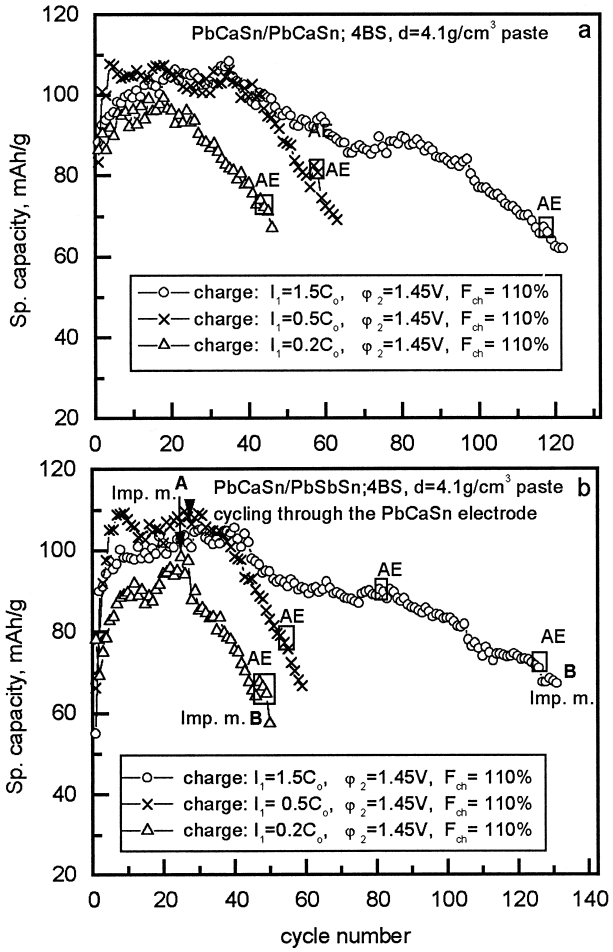

Fig. 3. Evolution of electrode capacity on cycling of (a) symmetrical electrodes and (b) asymmetrical electrodes with charging currents 1.5, 0.5 or $0.2C_0$ A. The potential transients on charge of these electrodes under the three charging modes are presented in Fig. 4. The capacities delivered through the AE are enframed.

Second, the longest life cycle of the MBE is of the order of 120 cycles. This is a life cycle shorter than that of the positive plates under compression in the lead–acid battery. This is an evidence that the destructive phenomena have indeed manifested in full and relatively quickly in the MBE where the PAM expands freely on cycling.

The evolution of the potential transients (E/t) on cycling of the symmetrical electrodes are presented in Fig. 4a–c and for asymmetrical ones in Fig. 4d–f.

An analysis of the potential transients in Fig. 4 indicates the following.

The transient profile depends on the current density and the number of cycles. On charge with $I_1 = 0.2C_0$ and $0.5C_0$ A, the potential curve features a maximum M_1 first (Fig. 4a, b, d and e). Then a plateau W follows, after which the potential increases reaching a value of 1.45 V. On charge with $I_1 = 1.5C_0$ A (Fig. 4c and f), a sharp peak P_1 appears first followed by a minimum and then the potential increases.

The quantities of electricity Q_1 flowing through the electrode for the time t_1 (Fig. 4a,d) under the different charging modes are as follows: $Q_1/Q_d \approx 80\%–85\%$ at $I_1 = 0.2C_0$ A; $Q_1/Q_d \approx 40\%–50\%$ at $I_1 = 0.5C_0$ A; and for the 10 min when charged at $I_1 = 1.5C_0$ A the electrode is charged only up to 16% of the Q_d. Q_d is the capacity of the preceding cycle. This indicates that the life cycle of the electrode is influenced by the first stage (I_1) of charge, when only a certain part (16%) of the electrode structure is formed. A critical part of the PAM structure (15%–20%) proves to be of essential importance for the life cycle of the positive plates.

At the end of life of the electrodes cycled at $I_1 = 0.5C_0$, the profiles of the potential transients evidence a small potential peak P_2 (Fig. 4b and e). When the P_2 peak is clearly pronounced, the maximum M_1 disappears and the capacity decreases (Fig. 4b, cycle 62; Fig. 4e cycles 49 and 52).

Fig. 5 shows the potential of the P_1 peak that appears at $I_1 = 1.5C_0$ A as a function of the number of cycles. The P_1 peak grows with increasing the number of cycles and after 80–100 cycles the slope of the P_1/cycles curve becomes very steep. This change in slope is related to the formation, during discharge, of a critical structure with higher resistance, which is accumulated in the electrode and hence leads to a fast decline in capacity of the plates.

The arrows in Fig. 3b indicate the cycles during which the impedance spectra were recorded after discharge of the asymmetrical electrodes down to 0.7 V at $I_1 = 0.2C_0$ or $I_1 = 1.5C_0$ A.

Fig. 6 presents the impedance spectra for the PbSnCa electrode spines with the corresponding equivalent circuit, which has given the best fit of the experimental data. Points are experimental values, solid line — fit according to the equivalent circuit presented in the figure. The equivalent circuit consists of two sub-circuits. The first one can be associated with the electrical parameters of the interface and the other one represents those of the PAM. The constant phase element Q_i has been taken rather than the pure capacitance element. R_{el} stands for the resistance of the electrolyte, R_1 denotes the resistance of the interface, Q_1 is the constant phase element representing the dielectric properties of the interface, Q_2 is the pseudo-Warburg impedance component, characterising the diffusion through a finite region of the interface, R_{ct} is the charge transfer resistance of the PbO_2/solution interface in PAM, Q_3 is a constant phase element representing the double layer capacitance at the PAM/electrolyte interface. The calculated values for R_1 and R_{ct} are also presented in the figure.

At the beginning of cycling, the electrode cycled with low initial charging current has slightly higher resistances R_1, R_{ct} than those for electrodes cycled at high charging current. On comparing the values of R_1 and R_{ct} at the end of life, it can be seen that the electrode charged at $I_1 = 0.2C_0$ A, though with a life cycle of only 45 cycles, has twice higher R_1 resistance and three times higher R_{ct}

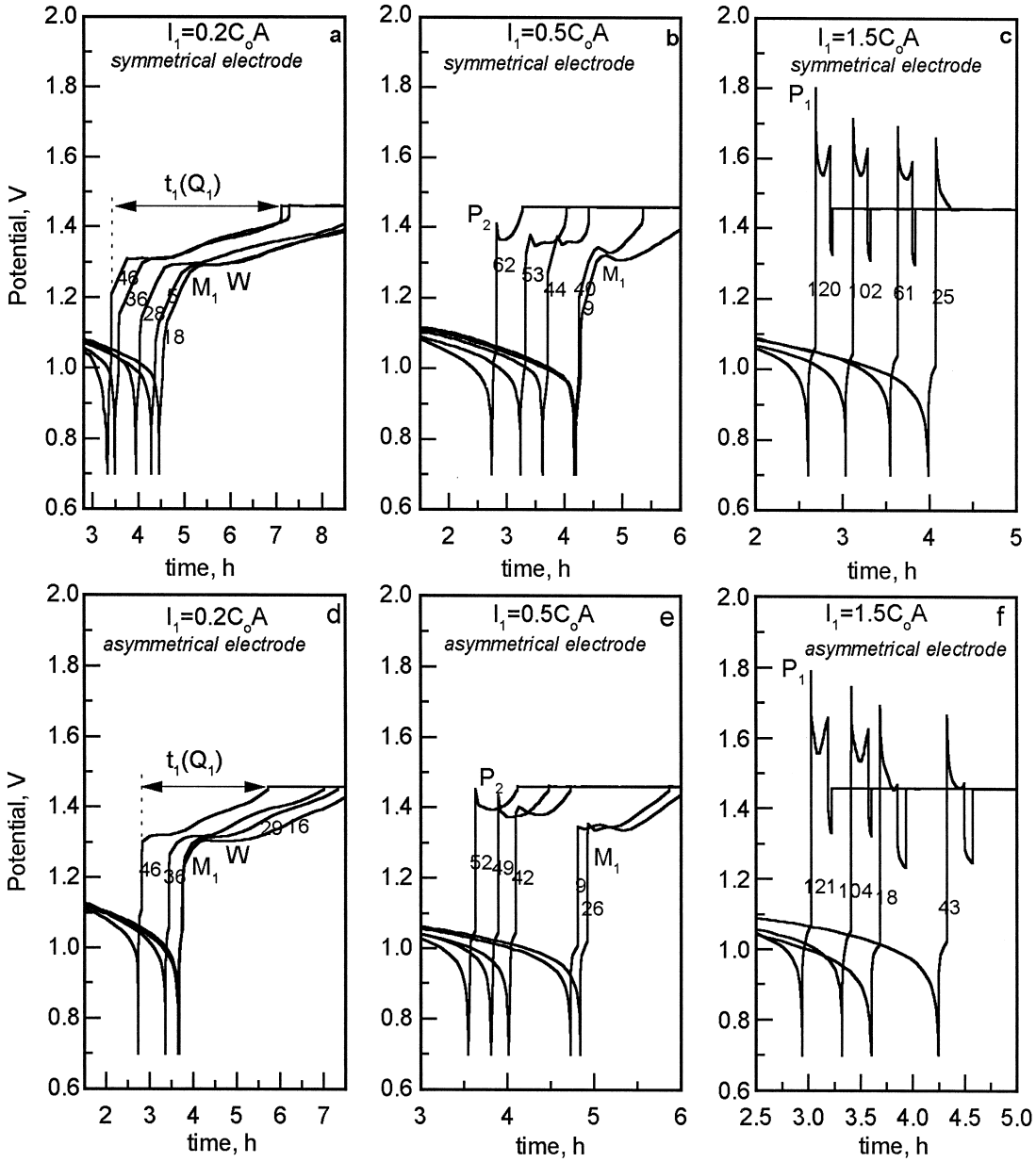

Fig. 4. Potential transients on charge of: (a,b,c) symmetrical electrodes; (d,e,f) asymmetrical electrodes under the three charging modes. The numbers on the transients give the number of cycles.

resistance as compared to those of the electrode charged at $I_1 = 1.5C_0$ A, which has a life cycle of 130 cycles. This difference in electron transfer resistance in the two electrodes charged at different currents indicates that the charging current affects the nature of the PAM and of the interface.

3.2. Dependence of electrode life cycle on current density

Fig. 7 shows the number of cycles until the electrode reached a specific capacity equal to 70 mA h/g (assumed for the end-of-life criterion) as a function of the current density during the first charge stage. The MBE's life cycle is a linear function of the current density during the first charge stage.

The results presented in Fig. 7 refer to MBEs discharged mainly through the PbSnCa spine. Only in individual cases the electrodes were subjected to several discharge cycles through the AE. The fact that the data for both symmetrical and asymmetrical electrodes lie on the same line indicates that the phenomena that determine the life cycle of the MBE proceed in the PAM. This conclusion is in agreement with the data in reference [7,8].

3.3. Initial electrode behaviour on cycling

The structures of PAM and of the interface are formed during manufacture of the positive plate. Let us call this

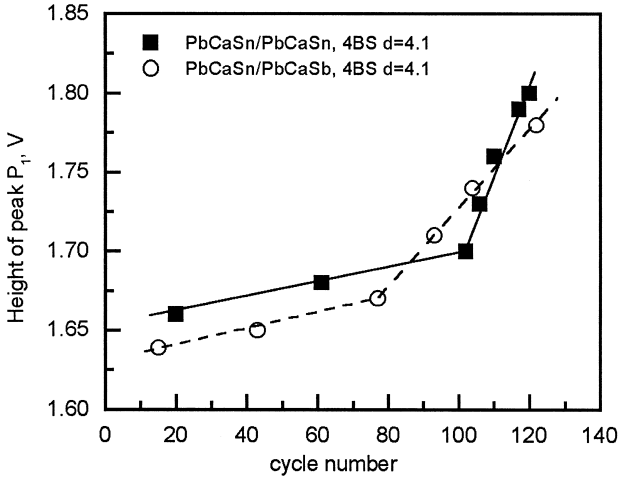

Fig. 5. Dependence of the height of peak P_1 (expressed in V) on the number of cycles for symmetrical and asymmetrical electrodes charged with $I_1 = 1.5C_0$ A. The rapid increase in height of the P_1 peak after 80–100 cycle is an indication of fast aging of the electrode.

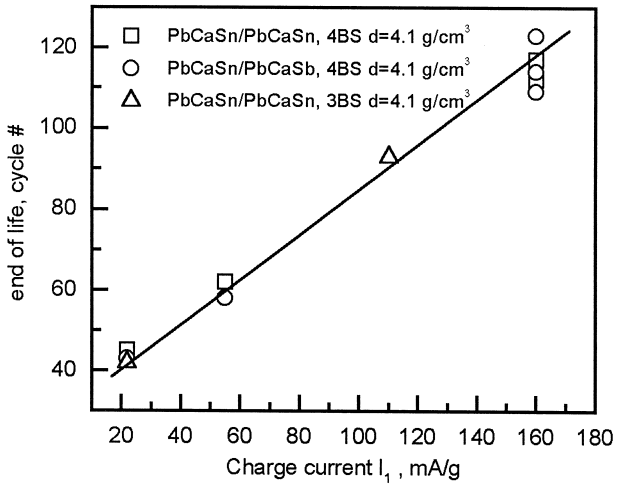

Fig. 7. Dependence of electrode life (in number of cycles until 70 mA h/g PAM) on current density during the first charge stage for symmetrical and asymmetrical electrodes.

structure ''technological''. It is formed as a result of oxidation of the basic lead sulphates, PbO and Pb. On cycling, up to 60% of the PbO_2 in the plate is involved in the charge–discharge processes. The structure of this part of PAM is formed as a result of oxidation of the $PbSO_4$. Let us call this structure ''operative''. During the first 10–15 cycles, the technological structure is converted into operative one.

Fig. 8 presents cycling curves for five MBEs cycled at $I_1 = 1.5C_0$ A (Fig. 8a) and five MBEs cycled at $I_1 = 0.2C_0$ A (Fig. 8b and c). All electrodes were cycled through the PbSnCa spine only. Based on the cycling curve profiles, the following structure types can be distinguished.

3.3.1. Normal structure

The capacity curves evidence a life cycle of about 120 cycles at $I_1 = 1.5C_0$ A and about 45 cycles at $I_1 = 0.2C_0$ A, respectively. The life of these electrodes is a linear function of I_1 (Fig. 7).

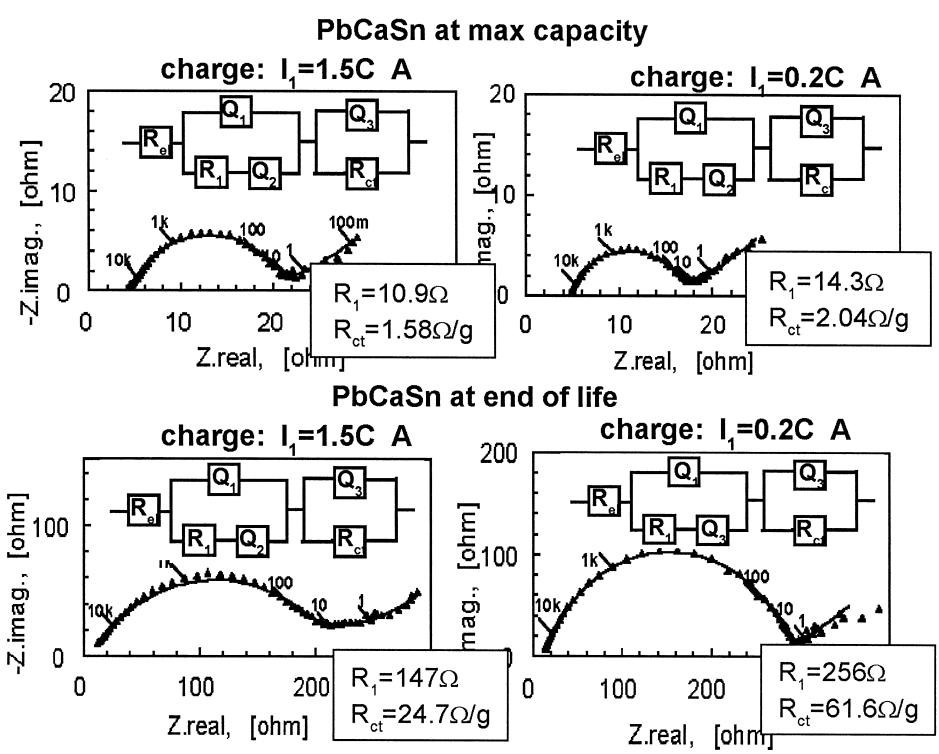

Fig. 6. Impedance spectra for discharged PbCaSn|PbSbSn MBE recorded at the beginning and at the end of life of the electrodes (i.e., at the cycles denoted as (A) and (B) in Fig. 3). All measurements were performed through the PbSnCa spine.

3.3.2. PCL effect facilitating structure [1]

The capacity curves evidence a rapid decline in the first 10 cycles. This is observed with one electrode cycled at $I_1 = 1.5C_0$ A (Fig. 8a) and two electrodes cycled at $I_1 = 0.2C_0$ A (Fig. 8b). Fig. 9 presents the potential transients for the two modes of charging of electrodes affected by the PCL effect. The following characteristic features can be observed: a potential arrest or a shoulder appears between 1.0 and 0.7 V in the discharge curve, whereas the charge curve features the peak P_3 and the maximum M_1 disappears (Fig. 9b, cycles 7 and 8). In the literature, a potential arrest in the cathodic curve on reduction of PbO_2 is related to the formation of non-stoichiometric lead oxides PbO_n ($n < 1.5$). The solution in the interior of the plate at the interface is alkalised [15] and the discharge proceeds until the formation of PbO_n [16] according to the E/pH diagram [17]. When the stoichiometric coefficient becomes smaller than 1.5, the resistance of the non-stoichiometric oxide increases by 8–9 orders of magnitude [18]. PbO_n phases with $n = 1.06$, 1.15, 1.60 have been identified in the interface through EPMA analysis [19].

The P_3 peak is due to the resistance of the PbO_n layer. On charge, PbO_n is oxidised to PbO_2 with a very small amount of electricity flowing. This means that the PbO_n layer is very thin. With oxidation of PbO_n to PbO_2 the electrode potential declines. As established in [20], the smallest cross-section through which the current flows in the plate is the interface corrosion layer/PAM. Hence, even the smallest changes in skeleton cross-section or in resistance of this interface will have a strong effect on the current flow in the plate and may limit the discharge of the plate. On charge, at the high potentials of the P_3 peak, oxygen and OH radicals are evolved at the interface, which oxidise PbO_n to PbO_2 and consequently, the potential declines.

The maximum M_1 occurs at the beginning of charge, when considerable amounts of current flow through the plate. Hence, this maximum reflects the oxidation of considerable zones both in the interface and in the adjacent PAM zones, in which the resistance increases on discharge. This high resistance limits the discharge.

A kind of competition could be expected between the processes of formation of the PbO_n layer and of the zones of high resistance in PAM during discharge. This competition depends on the structure of the plate at the interface. When this structure facilitates the formation of a thin PbO_n layer (Fig. 9), which limits the capacity before the formation of zones of high resistance, the M_1 peak does not appear. The case illustrated in Fig. 4a, b and d is different. These figures show that only the M_1 peak occurs during the initial cycles, i.e., the zones of high resistance at the

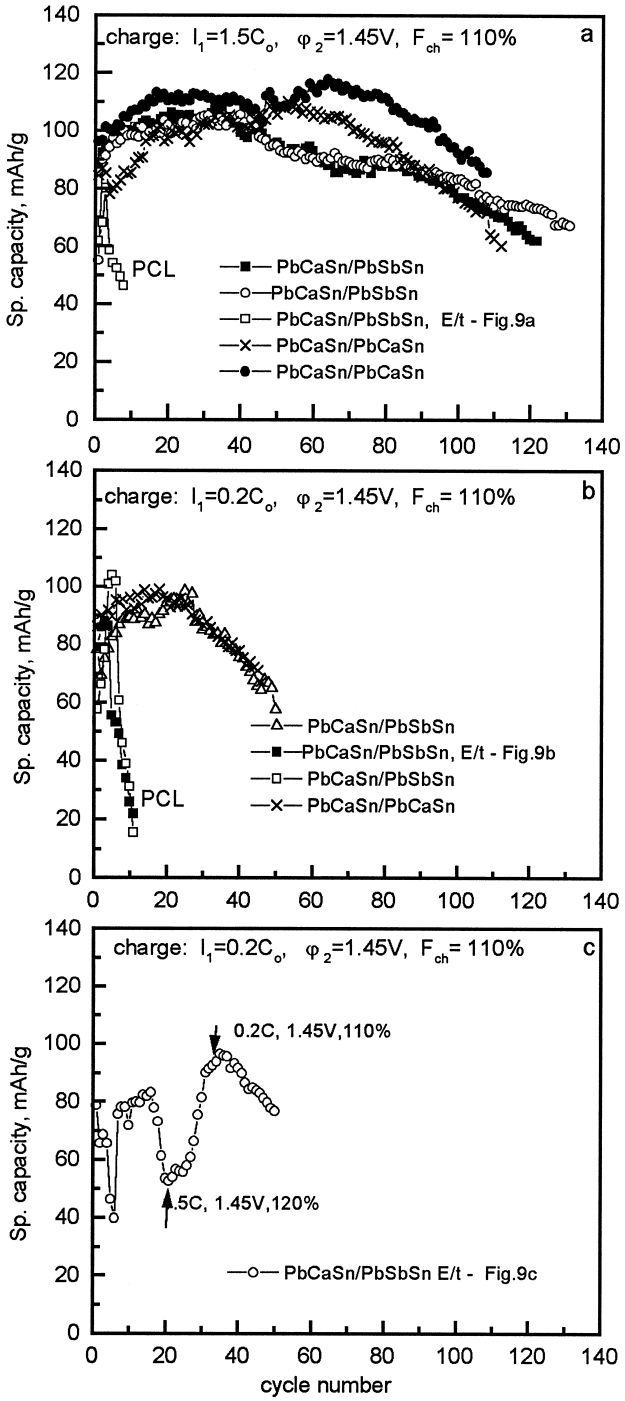

Fig. 8. Capacity curves on cycling of symmetrical and asymmetrical electrodes: (a) charging current $I_1 = 1.5C_0$ A. Four electrodes have normal structure and one has PCL facilitating structure; (b) charging current $I_1 = 0.2C_0$ A. Two electrodes have normal structure and two have PCL facilitating structure; (c) charging current $I_1 = 0.2C_0$ A. The electrode has metastable structure.

[1] The term PCL is used in this work to indicate the cases when the premature capacity loss is due to phenomena that occur at the interface. H. Giess denotes these cases by PCL-I to distinguish them from the PCL-II cases, when the capacity is limited by structural changes in PAM. The classification proposed by H. Giess has been adopted by the ALABC.

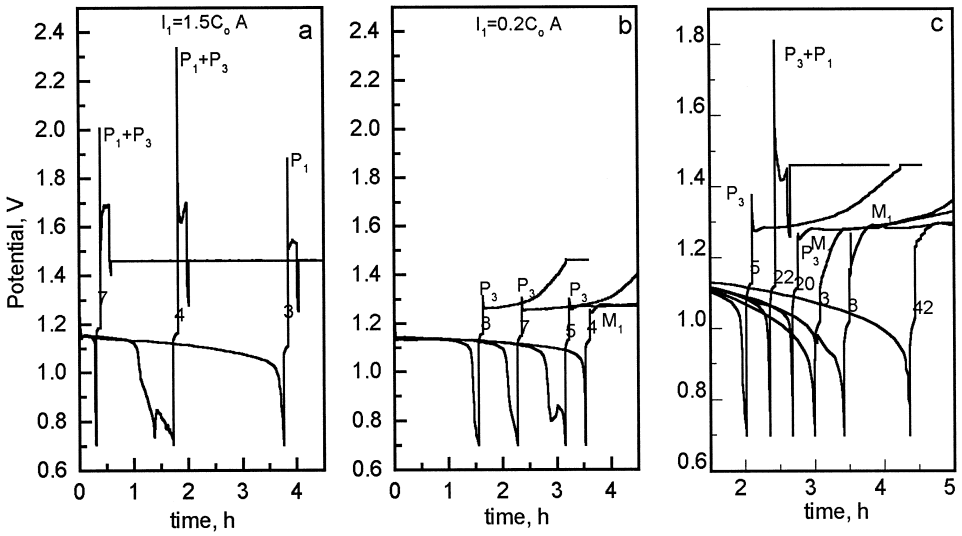

Fig. 9. Potential transients for electrodes with a PCL facilitating structure: (a) charging current $I_1 = 1.5C_0$ A. The capacity curve is presented in Fig. 8a; (b) charging current $I_1 = 0.2C_0$ A. The capacity curve is presented in Fig. 8b and is denoted with ■. The numbers on the transients give the number of cycles. (c) Potential transients for an electrode with metastable structure cycled at $I_1 = 0.2C_0$ A. The numbers on the transients give the number of cycles corresponding to the capacities presented in Fig. 8c.

interface alone limit the discharge. At the end of electrode life beside the M_1 peak also the peak P_2 occurs. Probably, its nature is similar to that of the P_3 peak. We have denoted these peaks with different numbers in order to point out that they are formed at different charge modes. Hence, at the end of life the capacity of the electrode is limited by both the PbO_n layer and the zones of high resistance.

3.3.3. Metastable structure

During the initial cycling period, this structure varies between the normal and the one causing PCL. The capacity curve for such an electrode is presented in Fig. 8c. When between 15 and 20 cycles the specific capacity declined down to 50 mA h/g, we changed the charging current to $I_1 = 1.5C_0$ A. Within the next 14 cycles, the capacity increased up to 90 mA h/g. Then the charging current was reduced to $I_1 = 0.2C_0$ A. Such an increase in capacity with increase in charging current was called RIMU [9].

Fig. 9c presents potential transients of some characteristic cycles of the electrode with metastable structure whose cycling curve is given in Fig. 8c. A potential arrest is observed between 0.85 and 0.7 V in the discharge curve at the 5th cycle and a pronounced P_3 peak (1.38 V). This is a behaviour typical of electrodes affected by the PCL effect. The specific capacity of the electrode is 45 mA h/g. When the capacity falls down again a potential shoulder occurs in the discharge potential transient (20th cycle) and the P_3 peak appears on charge together with the M_1 peak. When a charging current $I_1 = 1.5C_0$ A is applied (cycle 22), the potential peak P_1 is added to the P_3 peak giving a total peak height of 1.80 V, a value

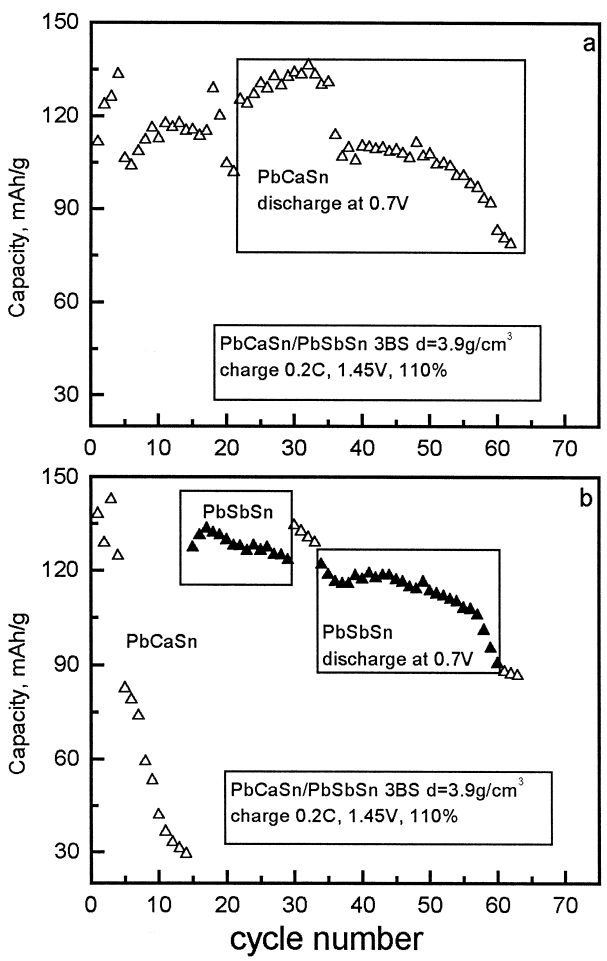

Fig. 10. Capacity curves for the two asymmetrical electrodes: (a) electrodes with normal structure; (b) the electrode has normal structure when cycled through the PbSnSb spine and PCL facilitating structure when cycled through the PbSnCa spine.

higher than that presented in Fig. 5 for electrodes with normal structure. It can be concluded that the interface structure is involved in the processes that occur at the end of discharge and at the beginning of the subsequent charge cycle.

The above three types of life cycle curves: normal, PCL structure and metastable structure are observed with low-antimony and antimony-free electrodes. Similar types of curves have also been registered on cycling of plates with pure Pb grids [21].

3.4. Formation of a barrier layer and influence of antimony on electrode behaviour

Fig. 10 presents the life cycle curves for one electrode with normal structure and one affected by the PCL effect. The electrodes were prepared with 3BS paste of a density $d = 3.9$ g/cm^3 and the cells were subjected to cycling at a charging current $I_1 = 0.2C_0$ A.

As evident from Fig. 10a, the life cycle of the electrodes with normal PAM structure reaches up to 62 cycles. It can be seen from Fig. 8 that, when produced with 4BS paste (density $d = 4.1$ g/cm^3), the cycling life of the electrodes, under the same conditions, is about 45 cycles. Hence, both the paste density and the origin of PAM (3BS or 4BS) influence the life of the electrodes on cycling.

The following investigations were performed aimed to attack the interface on discharge. When the electrode potential reached 0.7 V, the discharge was continued at this potential for 3 h. We assume that under the above conditions, the interface and the adjacent PAM zones are discharged. These cycles are enclosed in a frame in Fig. 10a.

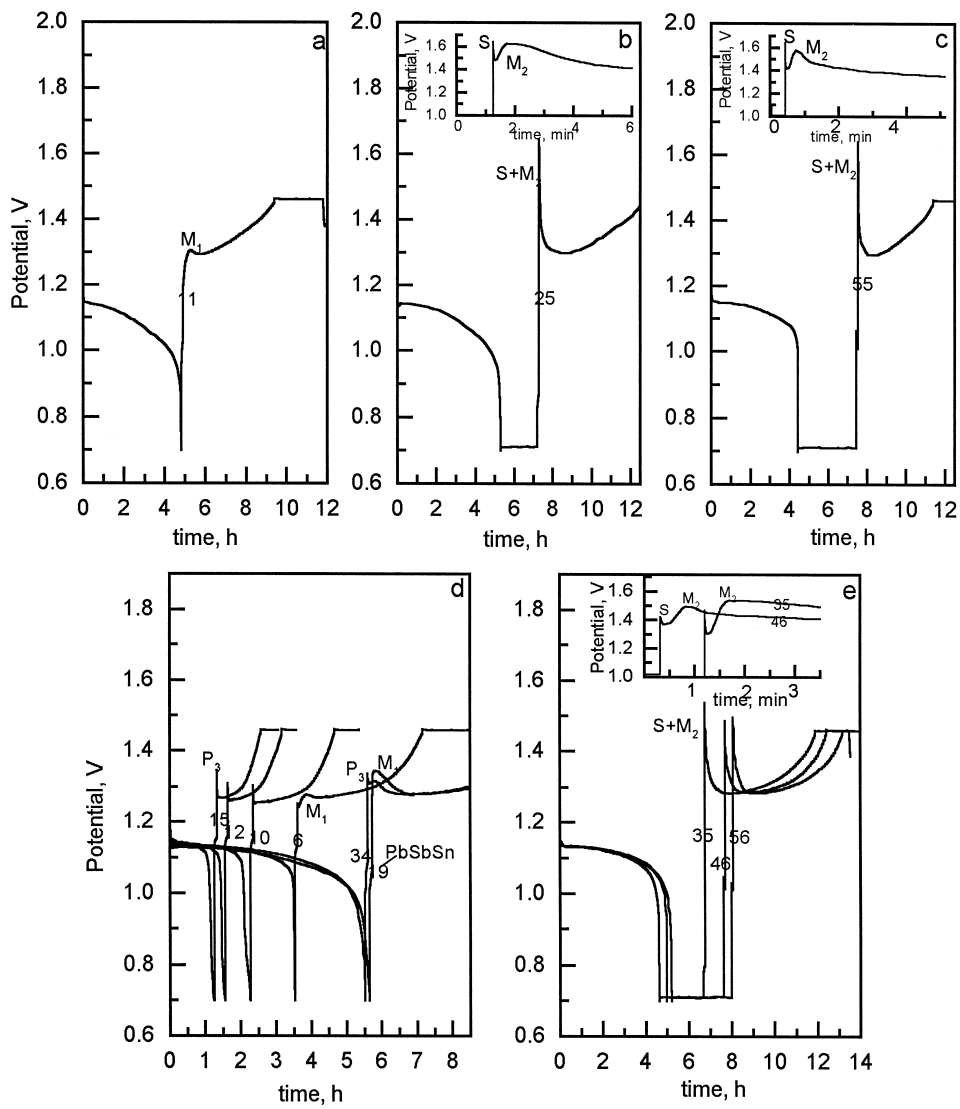

Fig. 11. a,b,c. Potential transients on charge and discharge (cycles 11, 25 and 55) of the asymmetrical electrode whose capacity curve is given in Fig. 10a. The peak $(S + M_2)$ in (b) and (c) is a composite peak and is shown in the insertions. It comprises the spike S and the maximum M_2. Fig. 11d,e. Potential transients on charge and discharge of the electrode whose capacity curve is given in Fig. 10b. The peak $(S + M_2)$ in (e) is a composite peak and is presented in the insertions in minute scale.

Fig. 11a–c present the potential transients on discharge and charge during the 11th, 25th and 55th cycles. The insertions in Fig. 11b and c show the peak S and the maximum M_2 at a magnified time scale (in min).

The transient at the 11th cycle (Fig. 11a) is typical of the charge and discharge of an electrode with normal structure and features a well shaped maximum M_1. When, during discharge, the electrode is polarized at 0.7 V for 3 h (Fig. 11b,c), the charge curve features a spike S and a maximum M_2. The spike implies that on polarization at 0.7 V a barrier layer is formed which is oxidized at higher polarizations for a short time period (very thin layer is oxidized), as a result of which the potential declines abruptly, after which the maximum M_2 appears. The formation of a barrier layer does not affect the life of the electrode. Probably, this is a very thin PbO or PbO_m $(1 < m < 1.3)$ layer which is formed at the interface Pb alloy/corrosion layer. PbO (or PbO_m) has a specific resistance of 10^{10} Ω^{-1} cm^{-1} [18]. The barrier layer causes the discharge current to decrease rapidly at 0.7 V polarization and further decay of the interface structure is slowed down or stops altogether. Thus, the barrier layer plays the role of a safety valve during discharge.

The maximum M_2 is probably of the same nature as the M_1 maximum, i.e., it is caused by zones of high electrical resistance formed in the PAM near the interface. (We have marked the two maxima with different numbers to point out that they are formed under different charging conditions.)

Fig. 10b shows the life cycle curve for an MBE affected by the PCL effect. The capacity decreased to 28 mA h/g for 14 cycles. Further cycling was continued through the PbSnSb spine. The behaviour of this electrode is similar to that of an electrode with normal structure. After 34 cycles, discharge through the PbSnSb spine continued for another 3 h at 0.7 V. The cycles during which the deep discharges were conducted are marked by a frame in Fig. 10b.

Fig. 11d presents the potential transients on discharge and charge of the electrode whose capacity curve is presented in Fig. 10b. It is cycled through the PbSnCa spine (cycles 6, 10, 12, 15 and 34) and through the PbSbSn spine (cycle 19). The behaviour of the curves up to the 15th cycle is typical of an electrode affected by the PCL effect, i.e., a potential arrest is observed in the discharge curve between 1.10 and 0.7 V and the peak P_3 appears.

At the 6th cycle, the M_1 peak is clearly pronounced and a very small P_3 peak appears. A tendency towards formation of PbO_n $(n < 1.5)$ oxides in the interface is observed. At the 10th, 12th and 15th cycles (Fig. 11d), the maximum M_1 disappears and the P_3 peak grows. Thus, on discharge, the formation of the PbO_n $(n < 1.5)$ layer proceeds at a higher rate than the formation of zones of high electrical resistance in PAM and hence the PbO_n layer becomes the capacity limiting parameter.

On further cycling of the electrode through the PbSnSb spine (19th cycle), the transient follows the profile of an electrode with normal structure (Fig. 11d), featuring a well pronounced maximum M_1. During the subsequent cycling

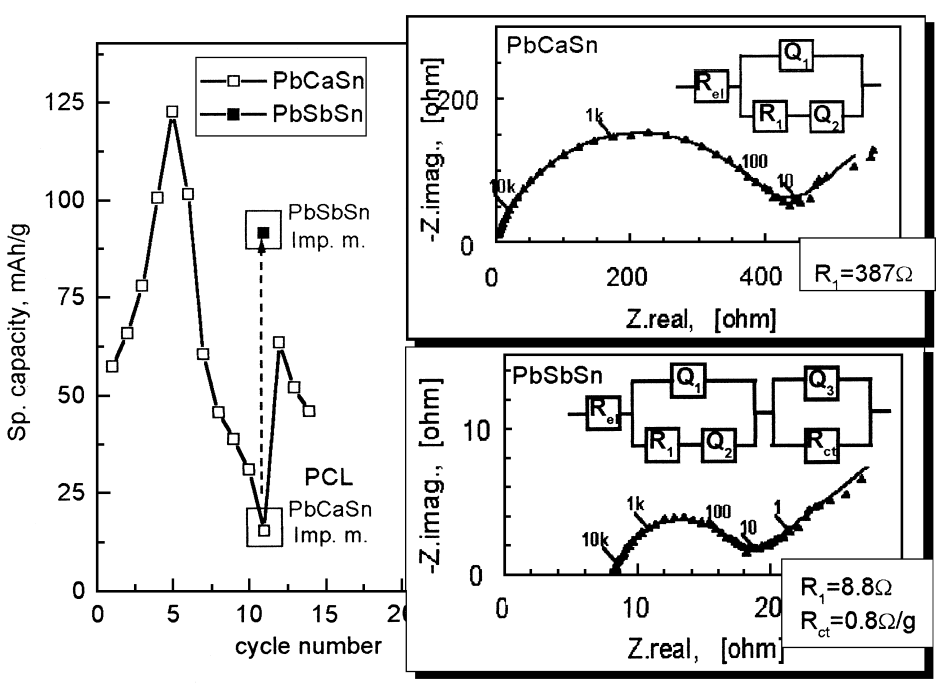

Fig. 12. Capacity curve for an asymmetrical electrode with provoked PCL effect. When cycled through the PbSnSb spine the electrode has normal structure and when cycled through the PbSnCa spine the PCL effect is manifested. The impedance spectra are recorded at the 11th cycle on discharge of the electrode through the PbSnCa and through the PbSnSb spine, and is presented in the insertion together with the equivalent electrical circuits of the discharged electrode.

through the PbSnCa spine (cycles 30–34) the PCL effect at the PbSnCa semi-electrode disappears and a small P_3 peak and M_1 maximum are observed. On cycling through the PbSnSb spine, the evolved antimony ions reach the PbSnCa spine and are incorporated into the structure of the interface and the adjacent PAM regions thus preventing the formation of a PbO_n structure. It has been established that antimony, even when uniformly distributed throughout the volume of the active mass, concentrates at the interface after a definite number of cycles [22]. This effect was related to the formation of complexes of the type $[SbOSO_4]^-$ and $[Sb_3O_9]$ [23]. These complexes prefer the pH of the solution in the pores near the interface. It has been established [24] that antimony slows down the rate of the discharge reaction $PbO_2 \rightarrow PbSO_4$. Hence, smaller amounts of $PbSO_4$ are formed in the interface layer. Moreover, antimony incorporated into the PbO_2 structure causes the potential of reduction of the $Pb_{(1-x)}Sb_xO_2$ mixed oxide to shift towards more negative values, as a result of which a smaller number of $PbSO_4$ crystals are formed in the interface [25,26]. Sb ions in $Pb_{(1-x)}Sb_xO_2$ increase the degree of hydration of PbO_2 leading to the formation of $PbO(OH)_2$ (gel zones), which reduce the formation of caverns and the mechanical cracking of the bridges between PAM and the current collector [27]. As a result of the above phenomena antimony reduces the probability of manifestation of the interface effects that are responsible for the occurrence of the P_1 and P_2 peaks.

Fig. 11e shows the potential transients during cycles 35, 46 and 56, when discharge of the electrode was continued at 0.7 V for 3 h aimed to see whether a barrier layer is formed at the interface PbSbSn/CL. A small spike *S* and a high maximum M_2 are distinguished. These are magnified in the insertion in Fig. 11e. These data indicate that Sb ions increase the conductivity of the lead oxides PbO_m, which explains the lower height of the *S* spike than that of the M_2 peak. Consequently, a greater amount of PbO_2 in PAM is involved in the current generation process and the end of discharge is limited by the formation of high-resistance zones at the interface.

3.5. Formation of $PbSO_4$ crystals in the interface and their role for the occurrence of the PCL effect

Fig. 12 shows the capacity curve for an electrode prepared with PbSnCa|PbSbSn|PAM (4BS with 4.1 g/cm^3 density of the paste). The initial five cycles were conducted with the PbSbSn and PbSnCa spines short-circuited during 10 h charge and discharge. The electrode capacity increased rapidly. The low initial capacity value and its rapid increase imply that the 4BS crystals had not been completely oxidized during formation and the process continued during the initial five cycles, as a result of which the specific capacity reached a value of 125 mA h/g. During this period, the technological structure was converted into operative one. The considerable increase in capacity implies that the structure has undergone substantial changes. It is interesting to see how much have these changes affected the two interfaces: PbSnCa/CL and PbSnSb/CL, respectively. Cycling of the electrode was conducted only through the PbSnCa spine between cycles 6 and 10 at a charging current of $0.2C_0$ A during the first charge stage. The capacity declined rapidly. The discharge during the 11th cycle was conducted first through the PbSnCa spine. The impedance spectra of the PbSnCa spine were recorded at the end of discharge. Then the electrode was discharged through the PbSbSn and the impedance spectra of the PbSbSn spine were recorded, too. The electrode capacity on discharge through the PbSnCa spine was 14.8 mA h/g and on discharge through the PbSbSn spine it was 94.5 mA h/g or the overall electrode capacity at the 11th cycle was 109.3 mA h/g. This result indicates that on conversion of the technological structure into operative one, a normal structure is formed in the PbSbSn/CL interface, whereas the PbSnCa/CL interface has a structure provoking the PCL effect, i.e., the two interfaces differ in behaviour. These results are similar to those obtained for double-grid plates [14].

Fig. 13 presents the potential transients on charge and discharge of the above electrode during cycles 4, 5 and 9. At the 4th cycle, though the electrode capacity is fairly high (125 mA h/g), the charge transient features beside the maximum M_1 also a small peak P_3. The presence of the latter peak is an indication of the electrode's inclination to the formation of PbO_n layer. The maximum M_1 implies that the formation of zones of high electric resistance in the interface determine the capacity and the phenomena causing the PCL effect have not manifested yet. The transient during the 9th cycle is typical of an electrode with PCL effect: potential arrest between 1.0 and

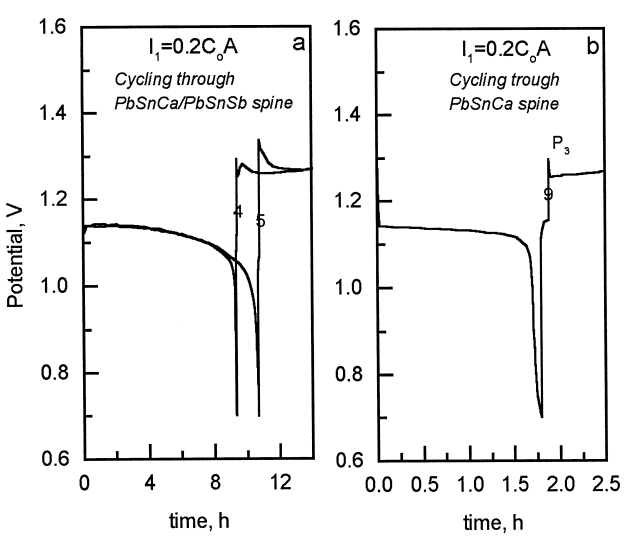

Fig. 13. Potential transients (at cycles 4, 5 and 9) for the asymmetrical electrode whose capacity curve is given in Fig. 12.

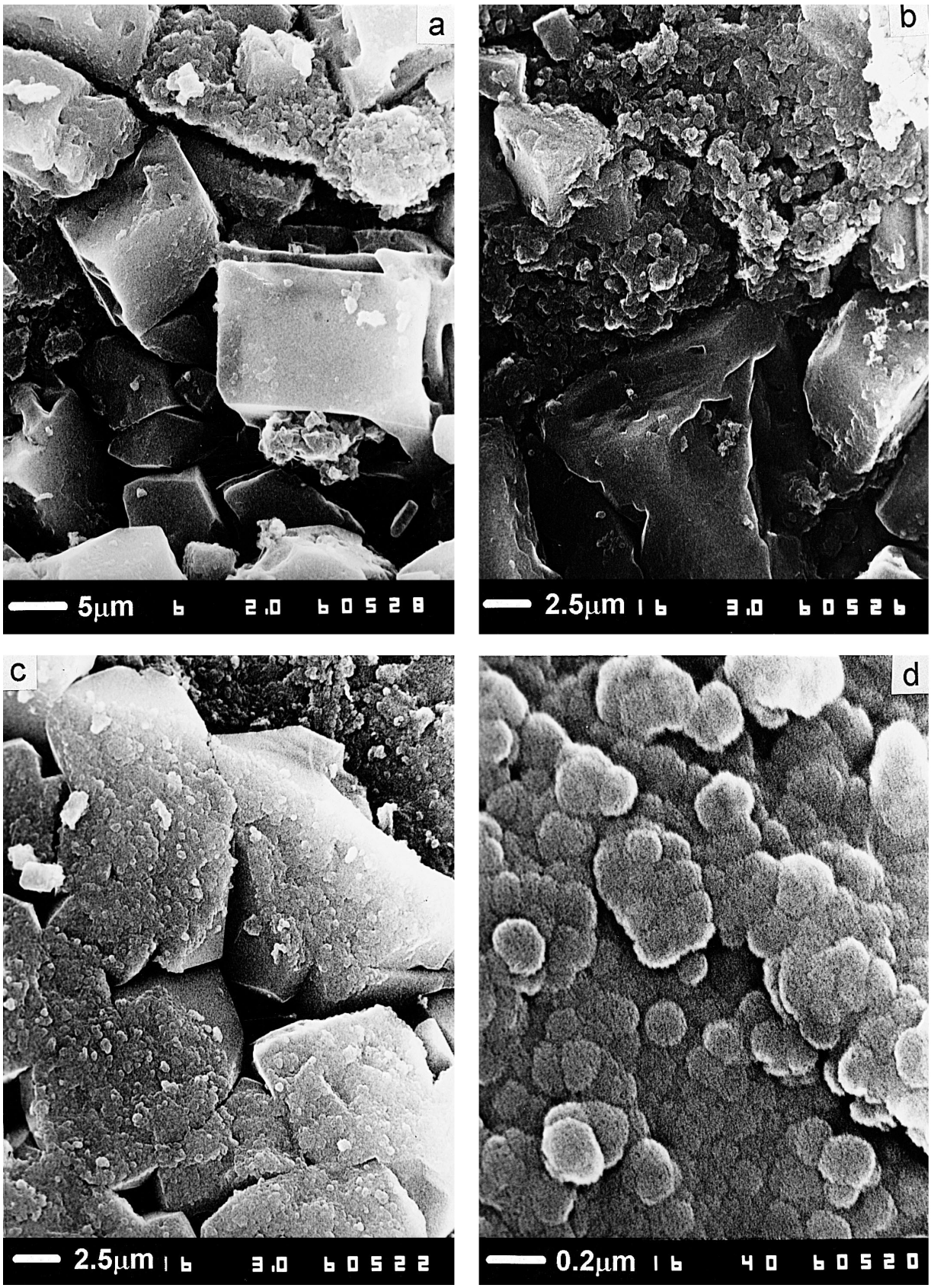

Fig. 14. SEM micrographs of the interface surface of the PbSnCa spine of the charged electrode. Many $PbSO_4$ crystals remain unoxidised while others are oxidised only on their surface. The obtained PbO_2 layer forms bridges between PAM and the compact part of the corrosion layer which facilitate the current transfer. Fig. 14d presents hydrated formations on the surface of the PbO_2 particles.

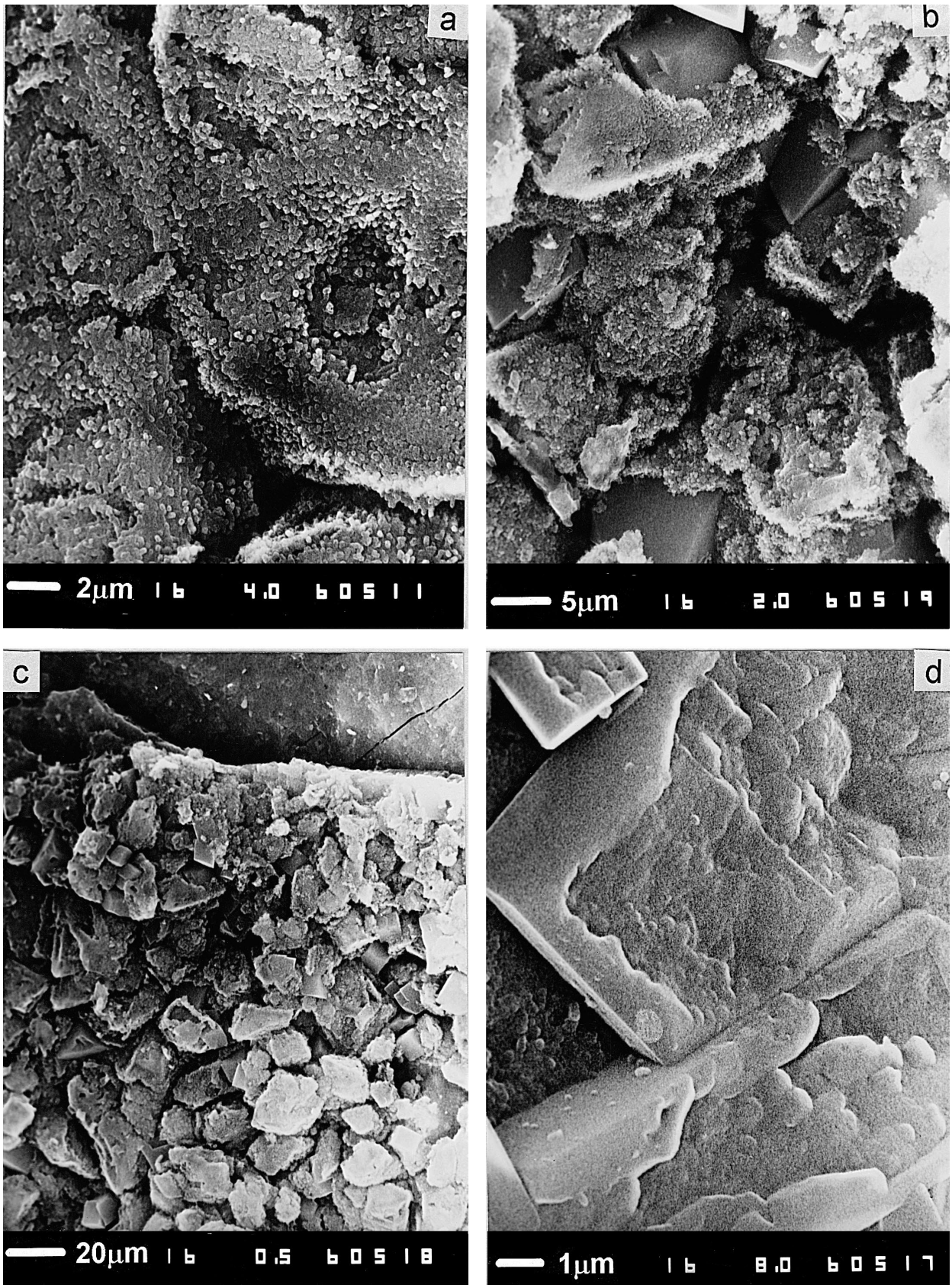

Fig. 15. SEM micrographs of the interface surface of the PbSnSb spine of the charged electrode. Many $PbSO_4$ crystals have been oxidised through a metasomatic process to form PbO_2 bridges.

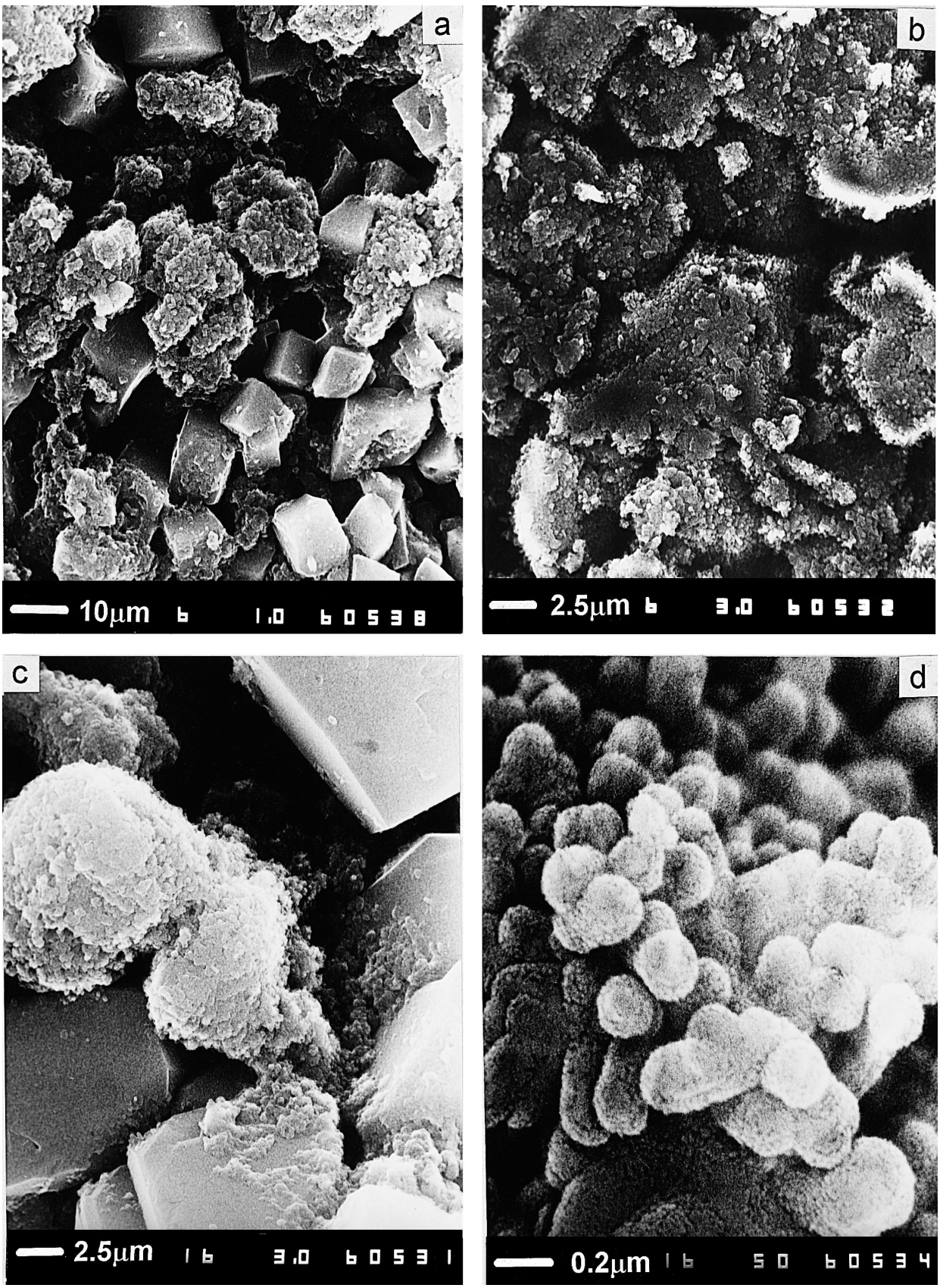

Fig. 16. SEM micrographs of the PAM surface at the interface close to the PbSnCa spine. Many $PbSO_4$ crystals have been oxidised through a metasomatic process. Unoxidised or partially oxidised crystals are also observed.

0.7 V on discharge and occurrence of a well pronounced P_3 peak. No M_1 maximum is observed in the potential transient on charge.

The obtained impedance spectra are presented in Fig. 12 with the equivalent circuit to which the impedance data was fitted. The data of the PbSnCa spine after discharge fit well the equivalent circuit representing the electrical parameters of the interface, whereas that of the electrode discharged through the PbSbSn spine features two sub-circuits: of the interface and of the active mass. On discharge of the electrode through the PbSnCa spine the capacity is limited by the high interface resistance $R_1 = 387\ \Omega$. When the MBE is discharged through the PbSbSn spine the interface resistance $R_1 = 8.8\ \Omega$ and charge transfer resistance of the PAM/solution interface have very low values, too. The impedance data support the conclusions drawn from the transients in Fig. 13.

We employed scanning electron microscopy (SEM) to find out the reason for the difference between the two interfaces. After the 14th cycle, the electrode was fully charged. It was taken out of the cell, washed with water and dried. Then, it was cut through so as to separate the active mass from the corrosion layers formed on the PbSbSn and the PbSnCa spines. The three interfaces were examined with a scanning electron microscope. Fig. 14 shows SEM micrographs of the surface of the corrosion layer formed on the PbSnCa spine. Though the electrode was fully charged, many unoxidised $PbSO_4$ crystals can be seen (Fig. 14a,b). Other $PbSO_4$ crystals are oxidised but only on their surface (Fig. 14c). The surface of the obtained PbO_2 particles covering the $PbSO_4$ crystals is shown in Fig. 14d (at magnification 40,000 ×). Rounded particles or agglomerates of interconnected particles are observed, which are typical of the process of formation of PbO_2 from the gel mass [28]. Under the action of the surface tension, rounded gel formations are obtained from the hydrated (gel) parts.

Fig. 15 presents SEM micrographs of the surface of the corrosion layer formed on the PbSbSn substrate. In this layer, too, unoxidised $PbSO_4$ crystals are observed, but these are much less in number than those observed in the corrosion layer formed on the PbSnCa substrate. Fig. 15d features $PbSO_4$ crystals that have been partly dissolved.

Fig. 16 shows SEM micrographs of the active mass at its interface with the corrosion layer formed on the PbSnSb surface. In this layer, too, $PbSO_4$ crystals that have not been oxidised to PbO_2 are observed (Fig. 16a,c). However, this layer features mostly PbO_2 agglomerates in which the matrix of the $PbSO_4$ crystals from which they have been oxidised is clearly outlined (Fig. 16a–c). At higher magnifications (Fig. 16d), rounded gel formations can be distinguished.

It has been found out that the $PbSO_4$ crystals formed at the interface are very difficult to oxidise and, if oxidised at all, these are the last $PbSO_4$ crystals in the plate to be converted into PbO_2 ones [29].

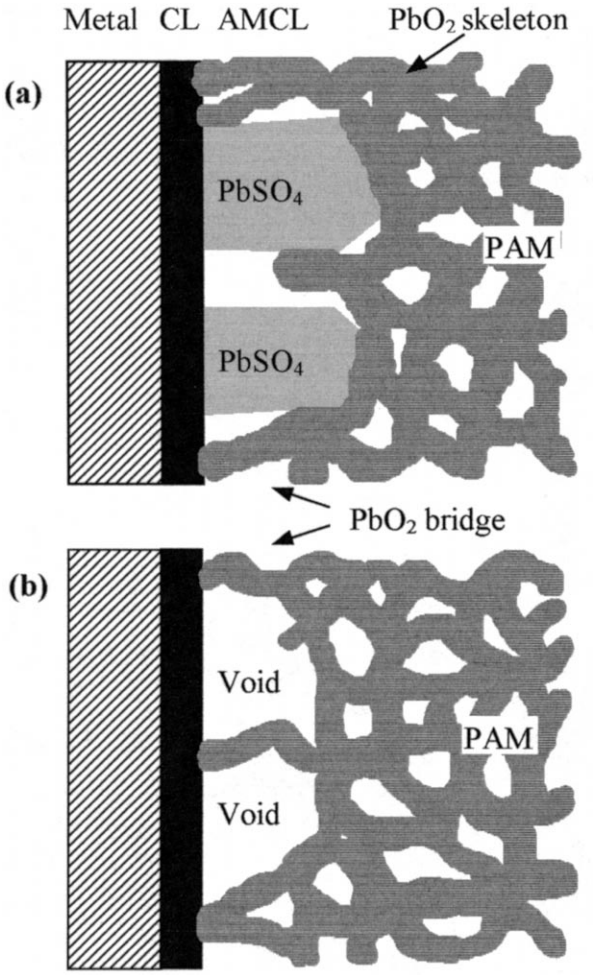

Fig. 17. Models for the interface of the PbO_2 electrode with PAM featuring $PbSO_4$ crystals (a) and caverns (b) in the interface.

An analysis of the data in Figs. 14–16 shows that the formation of $PbSO_4$ crystals in the interface that are hardly oxidised to PbO_2 is the reason for the PCL effect. These $PbSO_4$ crystals reduce strongly the number of bridges between PAM and the corrosion layer (Fig. 17a) as a result of which the current flow between PAM and the current collector is impeded. The formation of caverns and cracks in the interface has the same result (Fig. 17b).

4. Discussion

4.1. Heterogeneity of the macrostructure (skeleton) of PAM

Many authors have established that the discharge process does not proceed uniformly throughout the PAM volume. It has been shown that the PAM in the interior of the plate (about 1/3 of total PAM volume) does not take part in the discharge process during the first couple of cycles [15]. On further cycling, the pores in the outer parts

of the plate open thus allowing the active material in the plate interior to be involved in the current generation process. However, this does not lead to an increase in plate capacity because unfavourable structural changes take place in the active mass, which have an adverse effect on it dischargeability [15].

Other authors assume that on cycling, the PAM in the outer part consolidates into the coralloid structure and its utilization decreases [30]. This process opens up the pores in the structure in the outer part making the active material deeper inside the plate more accessible to the electrolyte and thereby increasing its utilization. This process continues until the PAM in the core is transformed into coralloid structure [30].

According to the above considerations, the heterogeneity of the plate is due to heterogeneity of the pore system. The different process rates may also be due to the difference in conductivity of the individual branches of the PAM skeleton. Some of these branches have a very small cross-section and others are highly hydrated (high ρ_{PAM}). Finally, the pulsation of the PAM skeleton on charge and discharge may create mechanical tensions in some of the skeleton branches, which may cause the skeleton to crack thus interrupting the current circuit in these branches.

As established earlier the PAM consists of:

(a) microstructure — lead dioxide particles interconnected into agglomerates with micropores in between [31,32];

(b) macrostructure — agglomerates interconnected into a skeleton with macropores between the branches [31,32];

(c) lead dioxide particles comprise crystal (PbO_2) and hydrated (gel) zones ($PbO(OH)_2$) [33].

Each of these structures has its own effect on the discharge process. On grounds of the processes that occur in the macrostructure, including the ionic processes that take place in the macropores, the bulk of PAM can be divided into separate zones (parts) in which the reactions proceed at different rates. These considerations should not be mixed up with the assumptions of the OAS model [9]. The latter is concerned with phenomena that take place on the microlevel, in the neck zone between two spherical particles. The present work is concerned with the macrostructure of PAM.

During galvanostatic discharge, the increased number of zones where the discharge reactions have been slowed down or have stopped altogether leads to an increase in current density in the other zones, where current generation proceeds. The cathodic polarisation of the electrode increases. The slope of the φ/t curves depends on the rate at which the different zones in the plate are excluded from the current generation process.

When more and more zones are excluded from the current generation process, or their contribution to this process is reduced, a moment will be reached when only a few zones will be involved in this process. Let us denote these zones with ''end-zones''. It is to be expected that these end-zones will be adjacent to (near) the interface. The current density in these zones will be high and so will be the polarisation of the electrode, which will increase with time and soon the cut-off voltage will be reached. The fact that the processes at the end of discharge are restricted to the regions near the current collector has been pointed out by many authors [6,34,35].

Let us now follow the processes that occur during charge of the PbO_2 plate, which is related to the aim of the present paper. The charge process will start first in the end-zones and, when the end-zones are charged and become electroconductive, the current generated in these zones will penetrate into the bulk of PAM. The current density in these zones will be the highest and the electrode will have the highest polarisation. When PbO_2 particles and agglomerates are formed and incorporated into the skeleton of the PAM and of the interface the contacts between the agglomerates will improve and new zones will be involved in the charge reaction. The current density will decrease and so will the potential of the electrode. Thus, the potential/time curve will feature a maximum at the beginning of charge. Its height and width will depend on the resistance and the number of end-zones, in which the charge reaction proceeds first. Figs. 4, 9 and 11 show this maximum in the potential curves marked as M_1 and M_2, respectively. This is the charge mechanism typical of the plates with normal structure where the end of discharge is limited by the resistance of the end-zones. This is the normal mechanism of the charge reactions in the macrostructure of the plate. However, a competing process proceeds in the interface, which is manifested by the peaks P_1, P_2, P_3 and S. These peaks are due to the abrupt decrease of the number of bridges between PAM and the corrosion layer as well as to the formation of PbO_n in the bridges. This process results in PCL effect. The above assumption for the essence of the PCL effect implies that a more precise term for this effect should be looked for. The term ''inefficient interface structure'' or ''interface effect'' would be more appropriate than the term ''PCL effect''. Moreover, that an objective criterion for this effect has been found, namely the peaks P_1, P_2 and P_3 in the charge curves. The case is different with the M_1 and M_2 maxima in the charge curves, which indicate that the discharge is limited by the high resistance of the end-zones in PAM.

4.2. Sol–gel–crystal mechanism of formation of the lead dioxide active mass

Most often the problems of PAM ageing and failure of the positive plate are related to expansion of the PAM and discontinuity of the PAM skeleton leading to a decrease in PAM conductivity [19]. The changes in electroconductivity of the PbO_2 skeleton on discharge are interpreted along the lines of the percolation theory and the effective medium theory [36,37]. The sharp fall in conductivity in the final

stage of discharge is due to the removal of a conducting pathway throughout the plate. These considerations are useful but they do not elucidate the nature of the phenomena that proceed on fast and slow charge, and their effect on the life cycle of the positive plates. Another approach to these phenomena is needed.

The processes on fast and slow charge are directly related to the rate of the electrochemical reaction and the chemical and crystallization processes invoked by this reaction. Hence, the question should be reduced to disclosing the effect of the kinetics of the electrochemical and chemical reactions on the structure of PAM formed on charge. Fig. 18 shows a scheme of the elementary reactions taking place during charge of positive plates, proposed by us earlier [38]. Below, we will discuss the specific features of the reactions according to this scheme.

4.2.1. Electrochemical reaction (3)

This reaction proceeds on the surface of PbO_2 particles and agglomerates. There the transfer of electrons from Pb^{2+} ions into the lead dioxide active mass takes place. The rate of the electrochemical reaction is determined by the outer power source. As a result of reaction (3), the composition of the solution in the pores and on the surface of the solid phase changes. As a result of this two types of processes occur: dissolution of $PbSO_4$ crystals (a reaction supplying the flow of Pb^{2+} ions into the pore solution) and formation of lead dioxide phase. Pb^{4+} ions are unstable in H_2O solutions and they react with water (reaction 4). The obtained H^+ ions (highly mobile) carry away the positive charges formed by reaction (3) from the pores to the bulk of the electrolyte.

4.2.2. Dissolution of $PbSO_4$ crystals

When the $PbSO_4$ crystals dissolve readily, the equilibrium between these crystals and the ions in the solution is maintained. The flow of electric current affects the undersaturation with Pb^{2+} ions in the pore solution in PAM and in the interface. At high charging currents, the undersaturation is greater and the $PbSO_4$ crystals dissolve rapidly. PbO_2 agglomerates are formed in sites different from the sites of $PbSO_4$ dissolution [38]. The size of the $PbSO_4$

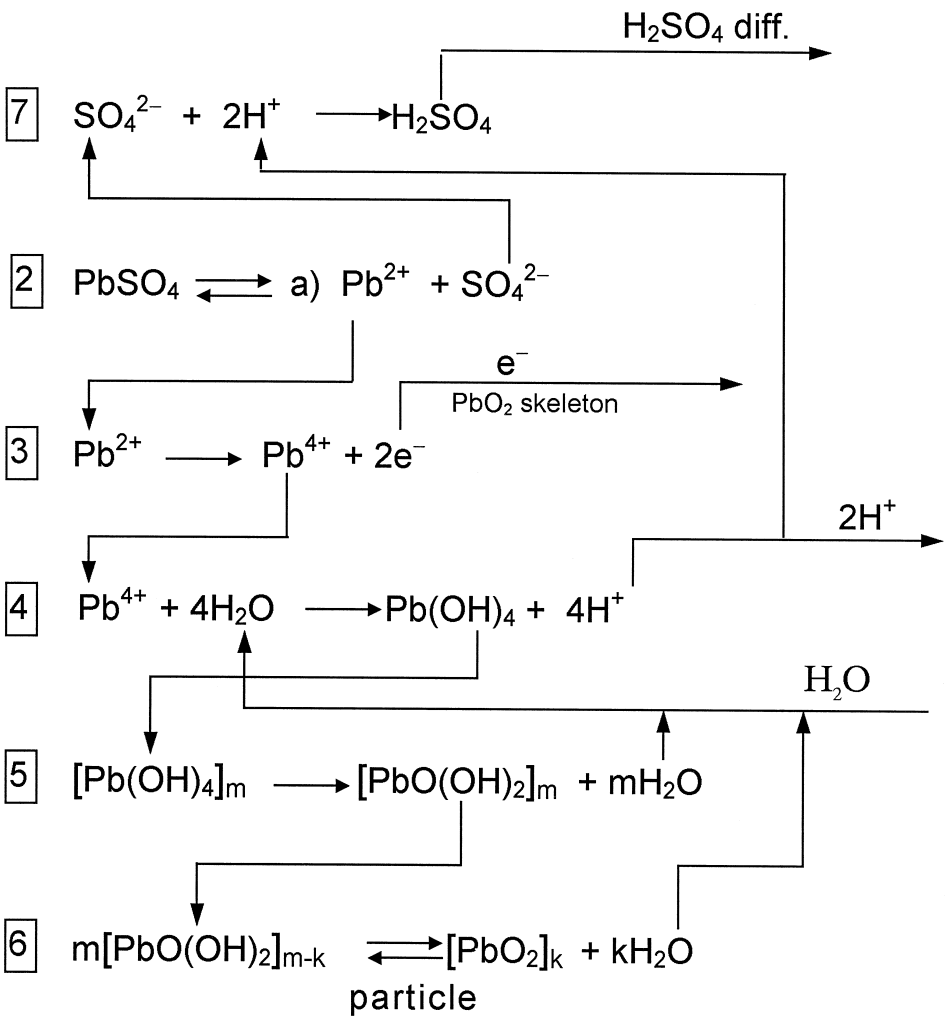

Fig. 18. Schematic representation of the elementary reactions involved in the charge process [38].

crystals formed during discharge does not affect the structure of PAM and of the interface.

When the $PbSO_4$ crystals are hard to dissolve, for one reason or another, the equilibrium (2) cannot be maintained and the ions in the solution are not enough for the reactions of PbO_2 formation (reactions 3 to 6) to proceed. The PbO_2 phase grows on the surface of the $PbSO_4$ crystals and a PbO_2 agglomerate is formed partially or completely within the matrix of the $PbSO_4$ crystals. This results in substantial changes in the microstructure of both the PAM and the interface. The $PbSO_4$ crystals are not always converted fully into PbO_2 agglomerates.

4.2.3. Chemical and physicochemical processes of lead dioxide formation

The $Pb(OH)_4$ formed as a result of reaction (4) is in the form of sol, which is dehydrated through reaction (5) yielding particles of a gel $(PbO(OH)_2)_m$. Reactions (4) and (5) proceed at high rates and that is why $Pb(OH)_4$ is not detected as a separate phase in the plate. However, soluble four-valent compounds have been found experimentally by many authors [38–43].

It can be expected that the concentration of the $Pb(OH)_4$ sol would affect the processes of dehydration (5) and (6), which would yield different micro- and macrostructures of PAM. At low charging currents, the sol concentration is low and hence formation of gel particles and their interconnection into agglomerates would proceed on some sites only. This would result in non-homogeneous macrostructure of PAM with thinner and thicker skeleton branches. Besides, the processes of dehydration (5) and (6) would proceed at a low rate, which would allow the obtained water to leave the agglomerates and a smaller number of micropores would be formed. At high charging currents, the sol concentration would be high. It would fill in all pores in the reaction zone and the newly formed agglomerates in PAM would be distributed more homogeneously. A more homogeneous PAM macrostructure would be formed. Moreover, due to the high rate of dehydration the obtained water would not have time enough to leave the agglomerates and hence a greater number of micropores would be formed. These would ensure higher capacity of the plates.

It can be concluded from all above said that the charging current density affects the formation of both the macrostructure and the microstructure of PAM. This, in turn, influences the capacity and the life cycle performance of the positive plates. To study the effect of fast and slow charge on PAM structure would be the aim of another paper.

4.3. Effect of charging current on the formation of the plate structure

When reaction (3) proceeds at a high rate (i.e., at high charging current) a high concentration of $Pb(OH)_4$ sol is obtained. The latter fills up the volume of the pores. Part of the $Pb(OH)_4$ is incorporated into the contacts between the agglomerates in the skeleton. Reactions (5) and (6) lead to the formation of some particles and agglomerates which are integrated into the skeleton and occupy part of the pore volume that has been vacated by the $PbSO_4$ crystals. Hence, a more compact skeleton is formed. Other particles are formed in the contacts between the agglomerates increasing the contact surfaces between them, as a result of which the electronic conductivity and mechanical strength of the skeleton of PAM and of the interface are improved. Thus, charging at high currents (fast charge) has a ''welding'' effect on the structure of the PAM and of the interface.

According to the concept of gradual exclusion of separate zones of PAM and of the interface from the discharge process (Section 4.1), during the subsequent fast charge the current will flow through a greater number of end-zones and hence a greater number of lead dioxide particles will be formed more homogeneously both in the interface and in the neighbouring PAM zones. The higher the current at the beginning of charge the greater the number of zones with high concentration of $Pb(OH)_4$ sol will be formed. Consequently, greater zones in the plate will have optimum micro- and macrostructure of PAM. Fig. 7 presents the linear dependence of the number of cycles on the current density during the first charge stage.

At low charging currents, the concentration of the sol is relatively small and PbO_2 particles and agglomerates are formed only in some parts of the interface and of PAM. The impedance spectra presented in Fig. 6 indicate that on cycling at $I_1 = 0.2C_0$ A, the structure of PAM changes in such a way that the electron transfer resistance in the electrochemical reaction (R_{ct}) increases several times as compared to the R_{ct} resistance of the electrode cycled at $I_1 = 1.5C_0$ A. This means that the sol concentration influences the nature of the particles and agglomerates formed during the charge reaction.

At low sol concentration, the effect of filling of contacts between the agglomerates with $Pb(OH)_4$ sol will be relatively weak. The skeleton features a definite number of weak and broken contacts as a result of which a greater number of zones will be excluded from the current generation process during the subsequent discharge. The ''welding'' effect in the structure of PAM and of the interface is weaker on slow charge. Besides, on slow charge the charge processes proceed in a small number of end-zones only as a result of which the heterogeneity of the macrostructure of the interface and of PAM increases. All these phenomena lead to shortening of the life cycle of the battery.

5. Conclusions

It has been established that the discharge of the lead dioxide electrode may be limited by: (a) formation of

PAM zones with high electric resistance at the interface, which are oxidised first during charge giving a maximum in the potential transient at the beginning of charge, which is related to the oxidation of $PbSO_4$ in the above zones; (b) formation of $PbSO_4$ crystals and/or caverns and cracks in the interface, as a result of which the number of bridges between PAM and the corrosion layer decreases; on alkalization of the solution in the pores on discharge the PbO_2 bridges in the interface are reduced to PbO_n $(n < 1.5)$ which has high resistance; the latter is oxidised first to PbO_2 giving a sharp peak in the potential/time transient.

It has been found that when during discharge zones of high resistance are formed in PAM, the structure of the plate is normal. When, however, the discharge is limited by the interface and a potential peak appears first on charge, the structure of the interface is ''inefficient'' and facilitates the PCL effect (PCL-I).

It has been established that the life of the lead dioxide electrode on cycling at CC-CV mode of charge and discharge at 25 mA/g PAM down to 0.7 V is a linear function of the charging current.

The effect of fast charge is explained by a sol–gel–crystal mechanism of the charge reactions. The high rate of the electrochemical reaction of Pb^{4+} formation leads to the formation of high oversaturations of the $Pb(OH)_4$ sol in the pores of PAM and of the interface, and rapid formation of $PbO(OH)_2$ gel particles which interconnect to form agglomerates. The impedance measurements have shown that the charge rate affects the nature of the lead dioxide particles and hence the electrochemical reaction. Parallel to the formation of new agglomerates, the $Pb(OH)_4$ sol also fill in the thinner or broken contacts between the agglomerates in the PAM skeleton. Thus, on fast charge the weak contacts in the PAM skeleton are ''welded''. Based on the processes involved in the sol–gel–crystal mechanism, the conclusion has been drawn that the charge current density affects both the micro- and macrostructure of the PAM.

Acknowledgements

The authors acknowledge gratefully the financial support for this work kindly provided by Japan Storage Battery, they also want to thank Dr. H. Giess for the useful discussions.

References

[1] U. Hullmeine, A. Winsel, E. Voss, J. Power Sources 25 (1989) 27.
[2] J. Bohmann, U. Hullmeine, E. Voss, A. Winsel, ILZRO Project LE-277, VARTA R&D Sentre, Final Report 1982.
[3] E. Meissner, E. Voss, J. Power Sources 33 (1991) 231.
[4] E. Meissner, H. Rabenstein, J. Power Sources 40 (1992) 157.
[5] E. Meissner, J. Power Sources 46 (1993) 231.
[6] W. Borger, U. Hullmeine, H. Laig-Horstebrock, E. Meissner, in: T. Keily, B.W. Baxter (Eds.), Power Sources 12 (1989) 131, Proc. 16, IPSS Bournemouth, 1988.
[7] M. Calabek, K. Micka, P. Baca, P. Krivak, V. Smarda, J. Power Sources 62 (1996) 161.
[8] M. Calabek, K. Micka, P. Baca, P. Krivak, V. Smarda, J. Power Sources 64 (1997) 123.
[9] A. Winsel, E. Voss, U. Hullmeine, J. Power Sources 30 (1990) 209.
[10] E.M. Valeriote, J.K. Nor, V.A. Ettel, Proc. 5th Intl. Lead/Acid Battery Seminar, International Lead Zinc Research Organization, Research Triangle Park, NC, USA, 1991, pp. 93–122.
[11] E.M. Valeriote, D.M. Jochim, J. Power Sources 40 (1992) 93.
[12] T.G. Chang, E.M. Valeriote, D.M. Jochim, J. Power Sources 48 (1994) 163.
[13] L.T. Lam, H. Ozgun, O.V. Lim, J.M. Hamilton, L.H. Vu, D.G. Vella, D.A.J. Rand, J. Power Sources 53 (1995) 215.
[14] M.K. Dimitrov, D. Pavlov, J. Power Sources 46 (1993) 203.
[15] S. Ikari, S. Yoshizawa, J. Electrochem. Soc. Jpn. 27 (E-186) (1959) 223, 243, 613.
[16] L.I. Ljamina, N.I. Korol'kova, K.M. Gorbunova, Elektrochimia 10 (1972) 394.
[17] S.C. Barnes, R.T. Mathieson, in: D.H. Collins (Ed.), Batteries, Vol. 2, Pergamon, Oxford, 1965.
[18] F. Lappe, J. Phys. Chem. Solids 23 (1962) 1563.
[19] A.F. Hollenkamp, J. Power Sources 59 (1996) 87.
[20] D. Pavlov, J. Power Sources 53 (1995) 9.
[21] R. Nelson, D.M. Wisdom, J. Power Sources 33 (1991) 165.
[22] M. Kosai, S. Yasukawa, S. Osumi, M. Tsubota, J. Power Sources 67 (1997) 43.
[23] J.L. Dawson, M.I. Gillibrand, J. Wilkinson, in: D.H. Collins (Ed.), Power Sources, Vol. 3, Oriel Press, Newcastle upon Tyne, UK, 1971, p. 1.
[24] Y. Okada, K. Takahashi, M. Tsubota, Proc. EVS 11 (1993) 28.
[25] T. Laitinen, K. Salmi, G. Sundholm, B. Monahov, D. Pavlov, Electrochim. Acta 36 (1991) 605.
[26] D. Pavlov, B. Monahov, J. Electroanal. Chem. 305 (1991) 57.
[27] B. Monahov, D. Pavlov, J. Electrochem. Soc. 141 (1994) 2316.
[28] D. Pavlov, J. Electrochem. Soc. 139 (1992) 3075.
[29] T. Takehara, J. Power Sources 30 (1990) 55.
[30] T.G. Chang, J. Electrochem. Soc. 131 (1984) 1755.
[31] D. Pavlov, E. Bashtavelova, J. Electrochem. Soc. 131 (1984) 1468.
[32] D. Pavlov, E. Bashtavelova, J. Electrochem. Soc. 133 (1986) 241.
[33] D. Pavlov, I. Balkanov, T. Halachev, P. Rachev, J. Electrochem. Soc. 139 (1989) 3189.
[34] T.G. Chang, in: K.R. Bullock, D. Pavlov (Eds.), Advances in Lead Acid Batteries, Vol. 84-14, Electrochem. Soc. Pennington, NJ, USA, 1984, p. 86.
[35] E. Bashtavelova, A. Winsel, J. Power Sources 53 (1995) 175.
[36] K.F. Euller, R. Kirchof, H. Metzendorf, J. Power Sources 5 (1980) 255.
[37] H. Metzendorf, J. Power Sources 7 (1982) 281.
[38] D. Pavlov, E. Bashtavelova, D. Simonsson, P. Ekdunge, J. Power Sources 30 (1990) 77.
[39] W. Feitknecht, A. Gaumann, J. Chim. Phys. 49 (1984) 135.
[40] L.V. Vanjukova, M.M. Isaeva, B.N. Kabanov, Dokl.-Akad. Nauk SSR 142 (1962) 377.
[41] M. Skyllas-Kazacos, J. Power Sources 13 (1984) 55.
[42] M. Skyllas-Kazacos, J. Electrochem. Soc. 128 (1981) 817.
[43] E. Hameenoja, T. Laitinen, G. Sunfholne, Electrochim. Acta 32 (1987) 187.